AGU PUBLICATIONS

JGR

Journal of Geophysical Research: Atmospheres

RESEARCH ARTICLE
10.1002/2015JD024208

Representing effects of aqueous phase reactions in shallow cumuli in global models

Ji Nie[1], Zhiming Kuang[2,3], Daniel J. Jacob[3], and Jiahua Guo[3]

[1]Lamont-Doherty Earth Observatory, Columbia University, New York, New York, USA, [2]Department of Earth and Planetary Sciences, Harvard University, Cambridge, Massachusetts, USA, [3]John A. Paulson School of Engineering and Applied Sciences, Harvard University, Cambridge, Massachusetts, USA

Key Points:
- A EDMF model can well reproduce the results of a LES embedded with idealized aqueous reactions
- The aqueous oxidation of SO_2 by H_2O_2 is relatively slow compared to the in-cloud residence time of air parcels
- Operator splitting between tracer transport and aqueous reactions leads to significant errors

Correspondence to:
J. Nie,
jn2460@columbia.edu

Citation:
Nie, J., Z. Kuang, D. J. Jacob, and J. Guo (2016), Representing effects of aqueous phase reactions in shallow cumuli in global models, *J. Geophys. Res. Atmos.*, *121*, doi:10.1002/2015JD024208.

Received 10 SEP 2015
Accepted 24 MAR 2016
Accepted article online 28 MAR 2016

Abstract Aqueous phase reactions are important, sometimes dominant (e.g., for SO_2), pathways for the oxidation of air pollutants at the local and/or global scale. In many current chemical transport models (CTMs), the transport and aqueous reactions of chemical species are treated as split processes, and the subgrid-scale heterogeneity between cloudy and environmental air is not considered. Here using large eddy simulation (LES) with idealized aqueous reactions mimicking the oxidation of surface-originated SO_2 by H_2O_2 in shallow cumuli, we show that the eddy diffusivity mass flux (EDMF) approach with a bulk plume can represent those processes quite well when entrainment/detrainment rates and eddy diffusivity are diagnosed using a conservative thermodynamic variable such as total water content. The reason is that a typical aqueous reaction such as SO_2 aqueous oxidation is relatively slow compared to the in-cloud residence time of air parcels in shallow cumuli. As a result, the surface-originated SO_2 is well correlated with and behaves like conservative thermodynamic variables that also have sources at the surface. Experiments with various reaction rate constants and relative abundances of SO_2 and H_2O_2 indicate that when the reaction timescale approaches the in-cloud residence time of air parcels, the errors of the bulk plume approach start to increase. Treating chemical tracer transport and aqueous reaction as split processes leads to significant errors, especially when the reaction is fast compared to the in-cloud residence time. Overall, the EDMF approach shows large improvement over the CTM-like treatments in matching the LES results.

1. Introduction

Moist convection plays a number of roles in atmospheric chemistry including vertical transport and turbulent mixing of chemical species, photochemistry (by altering the radiation field), lightning production of NO_x, wet removal, and aqueous phase reactions. The aqueous phase reactions are very important for some chemical species, a prominent example being sulfur dioxide (SO_2). SO_2 has major sources from fuel combustion, ore smelting, volcano eruptions, and oxidation of dimethyl sulfide (DMS) emitted by the marine biosphere. SO_2 can be oxidized in the atmosphere, producing sulfate aerosols that affect air quality, cloud nucleation, and climate [e.g., *Berg et al.*, 2011; *Ghan et al.*, 2012]. Because the aqueous phase oxidation of SO_2 by H_2O_2 and O_3 is much more rapid than the gaseous phase oxidation by OH, it dominates global sulfate aerosol formation (60%–80%) [e.g., *Barth et al.*, 2000; *Rasch et al.*, 2000; *Benkovitz et al.*, 2006; *Wang et al.*, 2011]. Thus, it is important to appropriately represent this type of aqueous phase reaction in global models.

In current chemical transport models (CTMs; and global climate models, GCMs, with chemistry components), due to their coarse resolution, shallow cumuli are parameterized, as are the associated aqueous phase reactions. In many CTMs [e.g., *Barth et al.*, 2000; *Liu et al.*, 2005; *Jöckel et al.*, 2006; *Verma et al.*, 2007; *Wu et al.*, 2007], the transport and reactions of chemical tracers are treated as split processes over a CTM time step: the CTMs first use the convective mass flux to calculate the convective transport then call chemical solvers to calculate the gaseous and aqueous phase reactions. In addition, the chemical solvers usually use the CTM grid mean chemical concentrations to calculate the aqueous phase reactions. The subgrid-scale heterogeneity (e.g., the difference between cloudy and clear-sky regions) of chemically reactive tracers and their correlations is not considered. The above two simplifications are justifiable for gaseous phase reactions that occur throughout a grid cell but are less justifiable for aqueous phase reactions. Aqueous phase reactions in cumuli

mainly occur in cloudy updrafts, in which the concentrations of chemical tracers can be quite different from the grid mean concentrations, as shown in both observations [e.g., *Daum et al.*, 1984] and numerical modeling [e.g., *Kazil et al.*, 2011]. The cloudy updrafts also contribute to the majority of the tracer transport above the subcloud layer [e.g., *Vilà-Guerau de Arellano et al.*, 2005], thereby coupling the chemical transport and reactions together.

The objective of this study is to improve representations of aqueous phase reactions in shallow cumuli in the global models, particularly to mitigate the errors due to the above two simplifications. We incorporate an idealized aqueous reaction into the large eddy simulation (LES) of shallow cumuli. LES has been used by many previous studies to investigate the effects of convection on chemistry, e.g., the photochemical disequilibrium in the dry boundary layer [*Krol et al.*, 2000] and the transport and transformations influenced by shallow cumulus [*Vilà-Guerau de Arellano et al.*, 2005; *Kim et al.*, 2012]. Here the LES resolves the turbulent flow and the aqueous reaction in the shallow cumuli at the cloud scale, which serves as the ground truth. The idealized chemical reaction is easy to understand and can be used as a starting point for the investigation of more complex chemical reactions in the future. We then assess whether a simple convective parameterization (the eddy diffusivity mass flux approach, EDMF, with a bulk plume model, simply called the EDMF model hereafter) with the aqueous reaction appropriately treated can well represent both the chemical and thermodynamic aspects at the same time.

Most convective parameterizations are designed to represent and are validated against the thermodynamic aspect of convection, such as heat and moisture, or inert chemical transport. Less evaluation has been done of the chemically reactive tracers, although the simulations of chemistry in global models are sensitive to the choices of convective parameterizations [e.g., *Jacob et al.*, 1997; *Easter et al.*, 2004; *Lawrence and Philip*, 2005]. To separate out the uncertainties in representing chemistry from the uncertainties in parameterizing convection and clouds themselves, we diagnose the parameters of the EDMF model from the LES results. The aqueous reaction is formulated within the EDMF model in a way that improves upon the above two simplifications (operator splitting and neglecting subgrid-scale heterogeneity of chemicals). We show that this representation of the aqueous reaction within the EDMF model can well reproduce the LES-simulated chemical aspect over a wide range of chemical regimes, thus making it an effective way to represent aqueous reactions and transport in shallow cumuli. We also analyze the errors of aqueous reaction in the EDMF model, which helps us understand and qualitatively assess when the EDMF model is adequately accurate and when it is not.

2. Methodology and Experimental Design

2.1. The LES With Reactive Tracers

The shallow cumuli case is the nonprecipitating oceanic trade cumulus case from the undisturbed Barbados Oceanographic and Meteorological Experiment (BOMEX) [*Holland and Rasmusson*, 1973]. The BOMEX shallow cumuli stayed in a steady state for 5 days in the field observation without apparent complications from precipitation or large-scale perturbations. It is an excellent test bed for us to focus on the chemical aspect, because the convective processes are relatively simple and well studied. The LES is the System for Atmospheric Modeling (SAM) [*Khairoutdinov and Randall*, 2003], which has been used to simulate the BOMEX case [e.g., *Siebesma et al.*, 2003; *Nie and Kuang*, 2012a]. We run SAM with a spatial resolution of 25 m in all directions in a domain of 6.4 km (x) × 6.4 km (y) × 3 km (z) with doubly periodic horizontal boundary conditions and a time step of 1 s. The forcing and other settings are the same as the intercomparison study of BOMEX described in *Siebesma et al.* [2003].

Two massless tracers, ϕ_1 and ϕ_2 with units of parts per billion, are added to the LES to mimic the aqueous oxidation of SO_2 by H_2O_2. ϕ_1 is released from the surface with a constant flux F_{sfc,ϕ_1}. ϕ_2, which mimics the atmospheric oxidant H_2O_2, is relaxed to a reference profile $\phi_{2,\mathrm{ref}}$ that is constant in height. We set the relaxation time of ϕ_2 to be 1 day based on photochemical production of H_2O_2 [*Jacob et al.*, 1990]. ϕ_1 is also relaxed to zero with a 1 day relaxation time, which may be viewed as representing gaseous phase oxidation, such as by OH [*Barth et al.*, 2000] or O_3 in sea-salt aerosols [*Alexander et al.*, 2005]. The relaxation of ϕ_1 and ϕ_2 is only applied in clear-sky grid cells. We limit this study to surface-originated ϕ_1, which may be viewed as anthropogenic sources of SO_2 or other pollutants. Other possible sources, such as the oxidation of DMS, will be considered in future work.

ϕ_1 and ϕ_2 react in cloud droplets within cloudy grids (grid cells with cloud liquid water $q_c \geq 0.01$ g kg^{-1}). The rate of the aqueous reaction can be expressed in their gaseous phase concentrations with a bulk reaction constant k

$$R_n = -\frac{d\phi_{1,n}}{dt} = -\frac{d\phi_{2,n}}{dt} = k\phi_{1,n}\phi_{2,n}q_{c,n}, \quad (1)$$

where the subscripts n indicate that they are for individual LES grid cells. k (with a unit of s^{-1} ppb^{-1} per g kg^{-1} of cloud liquid water; unit is omitted hereafter) is the product of the aqueous reaction rate constant in liquid water and Henry's equilibria constants (including the dissociation of SO_2 in the aqueous phase). The aqueous reaction rate constant is divided by the liquid water content, while the conversion from aqueous phase concentrations to gas phase concentrations is multiplied by the liquid water content. Thus, k in equation (1) has no dependence on $q_{c,n}$. For the aqueous oxidation of SO_2 by H_2O_2, k is about 1-2 $\times 10^{-3}$ [*Seinfeld and Pandis*, 1998]. Its dependence on the *p*H value is small and neglected. As in many previous studies [e.g., *Schumann*, 1989; *Vilà-Guerau de Arellano et al.*, 2005], the chemical reaction here is highly idealized. However, the minimal complexity of the chemistry allows us to better understand the influences of convection on chemistry and to improve its representation in parameterizations.

A control case is set up as the benchmark. The parameters F_{sfc,ϕ_1} and $\phi_{2,ref}$ determine the relative abundances of ϕ_1 and ϕ_2. In the control case, we set $F_{sfc0,\phi_1} = 0.024$ ppb kg m^{-2} s^{-1} and $\phi_{2,ref0} = 0.9$ ppb (subscript 0 indicates the control case value), so that the concentrations of ϕ_1 and ϕ_2 are comparable in cloudy updrafts. Observations show that either SO_2 or H_2O_2 can dominate depending on the environment [*Daum et al.*, 1984]. The control case k is set to be 10^{-3}, close to the representative value for SO_2 aqueous oxidation by H_2O_2.

To explore and evaluate the performance of the EDMF model in a wide range of situations, two groups of experiments are carried out in addition to the control case. Cases in group 1 have the same $k = 10^{-3}$ as in the control case. However, in each case $\phi_{2,ref}$ is divided and F_{sfc,ϕ_1} is multiplied by the same factor. There are a total of 12 cases with this factor varying from $\frac{1}{12}$ to 12. Experiments in this group cover SO_2 aqueous oxidation in different chemical regimes, from SO_2 dominant ($\phi_{2,ref}/\phi_{2,ref0} \ll 1$) to H_2O_2 dominant ($\phi_{2,ref}/\phi_{2,ref0} \gg 1$). In the second group of 12 experiments, we keep F_{sfc,ϕ_1} and $\phi_{2,ref}$ the same as in the control case but change k from 10^{-4} to 10^{-1}. Experiments in this group extend our study to explore a range of aqueous phase reaction rates.

The initial conditions of the chemical tracers are ϕ_1 being zero and ϕ_2 being its reference profile. For most of the paper, we focus on the comparison between the EDMF model and the LES results in the chemical steady state to remove the dependence on the initial conditions of chemical tracers. In section 3.6, we examine the first several hours after initialization to examine the EDMF model's performance in chemical transient state. Many LES, including SAM, can sustain a quasi-steady BOMEX convection only for several hours (hours 2–6 after the initialization; after that the thermodynamic fields slowly drift away) [e.g., *Siebesma et al.*, 2003], which is far less than the observed 5 days and too short to reach a chemical steady state without appropriate initial profiles of the chemical tracers. To overcome this limitation, we first run the model for 2 h. We then restart and run the model repeatedly from the end of hour 2 to the end of hour 6 from the same restart file (saved at the end of hour 2) except with a different set of Gaussian random noise applied to the temperature fields of the lowest five levels in each of the restarted runs. The added noise has a standard deviation of 0.02 K. ϕ_1 and ϕ_2 averaged over the clear sky and cloudy air are calculated at each height during the last hour of a previous run. Then, the clear sky and cloudy means are assigned as the initial values of ϕ_1 and ϕ_2 in the clear sky and cloudy air, respectively, of the following restarted run. We iterated this procedure for more than 12 rounds (48 simulation hours) for each case and confirmed that the chemical steady state is reached. Snapshots of thermodynamic (temperature T, total water content q_t, and others) and chemical variables (ϕ_1, ϕ_2, R) are saved every minute during the final run for analysis. The first 30 min simulation of the final run is discarded as spin-up, so that heterogeneities of ϕ_1 and ϕ_2 inside clouds and clear sky are fully developed for the analysis period.

2.2. The EDMF Model

The EDMF model is evaluated against the LES results. Consider the budget equation of an arbitrary tracer (ψ) horizontally averaged over the LES domain (denoted by overbar)

$$\frac{\partial\overline{\psi}}{\partial t} = \left(\frac{\partial\overline{\psi}}{\partial t}\right)_{forcing} - \frac{1}{\rho}\frac{\partial F_\psi}{\partial z} + \overline{S_\psi}. \quad (2)$$

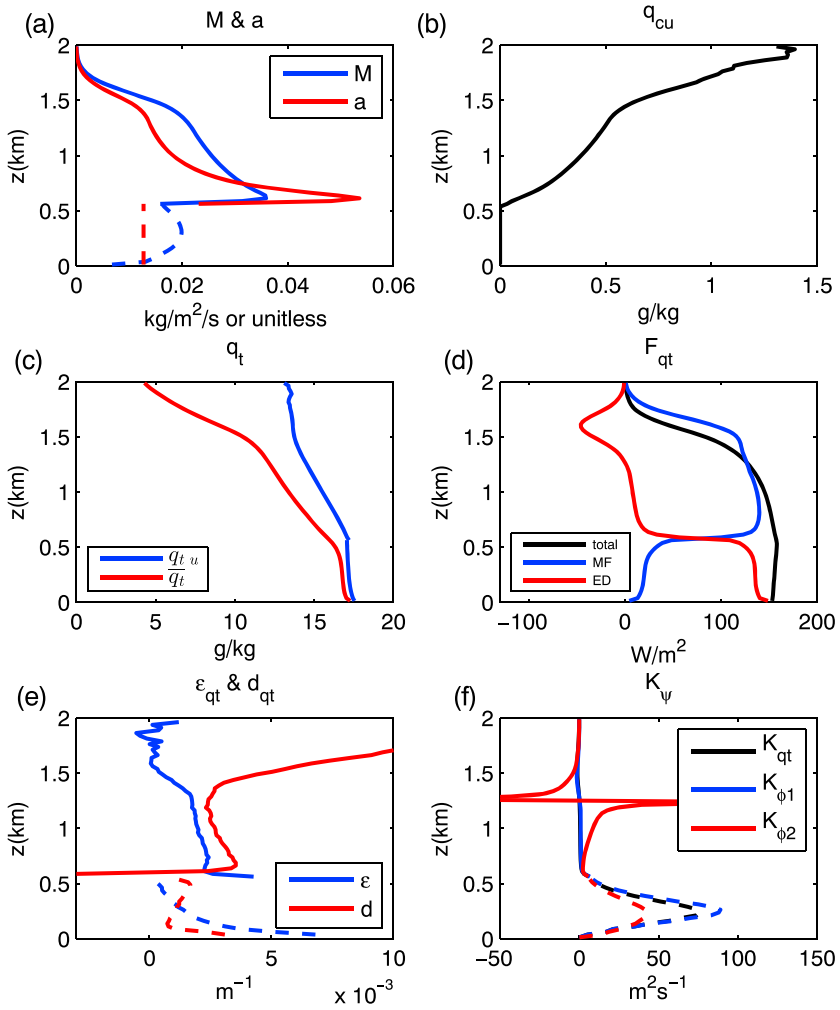

Figure 1. The LES-simulated (a) active updrafts area fraction a and mass flux M, (b) $q_{c,u}$, (c) total water content q_t in updrafts and environment, (d) F_{q_t} and its decomposition, (e) ϵ and d diagnosed form q_t, and (f) K diagnosed from q_t, ϕ_1, and ϕ_2. The dashed line indicates values in the subcloud layer.

ρ is air density. The terms on the right-hand side (RHS) are the imposed large-scale forcing, vertical convergence of turbulent flux, and net source, respectively. For the chemical tracers, the large-scale forcing term is zero, and the source terms include relaxation in the clear sky and the aqueous reaction in cloudy air.

By separating active updrafts from the environment [e.g., *Siebesma and Cuijpers*, 1995], the turbulent flux can be written as

$$F_\psi = \rho\overline{w'\psi'} = \rho a(1-a)(w_u - w_e)(\psi_u - \psi_e) + \rho a\overline{w'\psi'}^u + \rho(1-a)\overline{w'\psi'}^e, \tag{3}$$

where subscripts u and e indicate conditional averaging over active updrafts and the environment, respectively. w is the vertical velocity and a is the area fraction of active updrafts. Since a is very small for the BOMEX case (Figure 1a), we adopt the following highly accurate approximation in the rest of the paper: $(1-a) \approx 1$ and $\psi_e \approx \overline{\psi}$. The first term on the RHS of equation (3) represents net transport by active updrafts and the compensating subsidence. Under the above approximation, it can be written as $M(\psi_u - \overline{\psi})$, where $M = \rho a w_u$ is the convective mass flux. The second and third terms represent turbulent flux due to heterogeneities inside updrafts and the environment, respectively.

The EDMF model [e.g., *Siebesma et al.*, 2007; *Sušelj et al.*, 2012] parameterizes F_ψ as the sum of a mass flux (MF) component and an eddy diffusivity (ED) component,

$$F_\psi \approx M(\psi_u - \overline{\psi}) - \rho K_\psi \frac{\partial \overline{\psi}}{\partial z}, \tag{4}$$

where K_ψ is the eddy diffusion coefficient. To describe the MF component in the EDMF approach, we use a bulk plume model [e.g., *Siebesma et al.*, 2007]

$$\frac{1}{M}\frac{\partial M}{\partial z} = \epsilon_\psi - d_\psi, \tag{5}$$

$$\frac{\partial M\psi_u}{\partial z} = \epsilon_\psi M\overline{\psi} - d_\psi M\psi_u + \rho S_{\psi,u}, \tag{6}$$

where ϵ and d (m^{-1}) are the effective fractional entrainment and detrainment rates, respectively. In the cloud layer, the active updrafts are defined as cloudy grids with upward vertical velocity ($q_c > 0.01$ g kg^{-1} and $w > 0$ m s^{-1}). In the subcloud layer, they are defined as grids with w values in the top 1.3% percentile, which is within the range (1%–5%) suggested by *Siebesma et al.* [2003, 2007]. *Sušelj et al.* [2012] tested that the overall results of their EDMF model are fairly insensitive to the specified threshold of the percentile. The tracers in the updrafts have initial values at the lowest model level (z_1) as the horizontal mean added with an excess that scales with the surface flux ($F_{\text{sfc},\psi}$),

$$\psi_u(z_1) = \overline{\psi(z_1)} + \alpha\frac{F_{\text{sfc},\psi}}{\sigma_w(z_1)}, \tag{7}$$

where σ_w is the standard deviation of w and $\alpha = 1.06$ is a scaling parameter from *Siebesma et al.* [2007]. Given the ψ values at the lowest level, we can integrate equations (5)–(6) upward to have the ψ_u values on all levels. Compared to many other parameterizations that treat the cloud layer and the subcloud layer separately, the EDMF model has the advantage of providing a unified framework that connects the subcloud layer and the cloud layer smoothly. It has been operational in several GCMs and has shown significant improvements in the simulation of shallow clouds [e.g., marine stratocumulus and continental stratus, e.g., *Koehler*, 2005].

The prognostic variables of the EDMF model (equations (4)–(7)) are q_t and the liquid water static energy ($h_l = C_pT + gz - Lq_c$, where C_p is the specific heat at constant pressure and L is the latent heat of vaporization) for the thermodynamic aspect and ϕ_1 and ϕ_2 for the chemical aspect. The EDMF model requires specifying the parameters ϵ_ψ, d_ψ, and K_ψ for each tracer. One can diagnose these parameters by matching the LES and EDMF model results (i.e., collecting M, $\overline{\psi}$, and ψ_u from LES snapshots and solving equations (5)–(6) for ϵ_ψ and d_ψ, collecting F_ψ from the LES and solving equation (4) for K_ψ with $-\rho K_\psi\frac{\partial\overline{\psi}}{\partial z}$ treated as the residual). *Siebesma et al.* [2003] showed that because of the strong correlation between q_t and h_l, their tracer parameters are very close to each other. Our analysis confirmed their conclusion: the normalized root-mean-square error between ϵ_{q_t} and ϵ_{h_l} is about 20%. As many parameterizations in CTMs do not have parameters for individual tracers, we evaluate the EDMF model with the same set of parameters diagnosed from q_t for both thermodynamic and chemical tracers. By doing so, we are considering the scenario that the EDMF model can "perfectly" represent the thermodynamic aspects of convection and clouds; thus, any errors in the chemical variables are due to the parameter dependence on tracers and deficiencies in the representation of aqueous reaction.

2.3. Treatments of the Aqueous Phase Reactions in the EDMF Model and Current CTMs

Effects of the aqueous reaction are considered here only within cloudy updrafts (R_u, equivalent to $-S_{\psi,u}$ in equation (6) for the reactive tracers), given the reaction rate in cloudy downdrafts being small. In the EDMF model, R_u is calculated using variables in cloudy updrafts,

$$R_{u,\text{EDMF}} = k\phi_{1u}\phi_{2u}q_{c,u}. \tag{8}$$

In other words, the effect of cloudy/clear-sky heterogeneity on the aqueous reaction is explicitly represented. Moreover, the transport and reactions of reactive tracers are calculated simultaneously as we integrate the bulk plume upward; therefore, they are coupled. In addition, the mass exchange of reactive tracers between the environment and cloudy updrafts is through entraining/detraining mixing processes, which are deduced from and constrained by the thermodynamic tracer.

The above representation of aqueous reaction is more consistent with the real atmospheric processes. With the transport (equations (4)–(6)) and the aqueous reaction (equation (8)) parameterized, we can run the EDMF as a single-column model using equation (2). At each time step, equations (5)–(6) and (8) are first integrated upward to obtain ψ_u and $S_{\psi,u}$. Next, equation (4) gives the convective flux F_ψ. This information is then used in equation (2) to calculate the tracer mixing ratio profiles of the following time step. Since the parameters

(ϵ, d, and K) are diagnosed from q_t using LES results, the EDMF model will reproduce the LES q_t perfectly and h_l near perfectly. Thus, we only simulate the chemical tracers with the single-column model and compare them against the LES results. The EDMF single-column model has the same vertical grids as the LES and a time step of 4 s, due to the consideration of numerical stability and the representation of aqueous reaction.

Parameterizations in current CTMs usually treat the transport and reactions of chemical tracers in shallow cumuli as split processes. The tracer transport by sub-CTM grid-scale convection and chemical reactions is calculated in separate modules. Moreover, it is common to use the CTM grid mean tracer concentrations to calculate the aqueous reaction in cloudy air,

$$R_{u,\mathrm{CTM}} = k\overline{\phi_1}\,\overline{\phi_2}q_{c,u}. \tag{9}$$

To estimate the potential errors due to process splitting in many CTMs, we run the EDMF single-column model as if the transport and reaction are separate as in the CTMs. Over a CTM time step (Δt_{CTM}), we first calculate the tracer transport tendencies using the EDMF model without aqueous reaction then calculate the tracer tendencies due to aqueous reaction using equation (9). The profiles of ϕ_1 and ϕ_2 are updated using the total tendencies over Δt_{CTM}. Note that since we do not update tracer profiles during the split processes (as some CTMs do), the results do not depend on whether transport or aqueous reaction is calculated first. This is a more consistent comparison with the EDMF model. In section 3.5, the results from this setting are compared with the EDMF model with transport and aqueous reaction coupled.

3. Results

We start with some basic characteristics of the BOMEX shallow cumuli in the LES (Figure 1). The area fraction (a, Figure 1a) of the active updrafts is specified to be a constant (1.3%) in the subcloud layer and decreases with height in the cloud layer. In the cloud layer, the net mass flux M also decreases with height but less than a because w_u increases with height due to buoyancy acceleration. At the cloud base (around 550 m level), a and M are discontinuous due to the different definitions of updrafts applied in the subcloud layer and the cloud layer. Although not for the reactive tracers examined here, for other tracers with strong vertical gradients near the cloud base, this discontinuity may induce biases in the EDMF model. $q_{c,u}$ increases with height due to continuous condensation as cloudy updrafts rise (Figure 1b). The active updrafts are significantly moister than the environmental mean, especially in the cloud layer (Figure 1c). As cloudy updrafts rise, turbulent mixing continuously entrains environmental air into cloudy updrafts, pushing cloudy updrafts' properties toward the environmental air properties. Figure 1d shows the flux of total water, Fq_t, and its decomposition through equation (4). The convective flux of q_t is mostly due to the ED component in the subcloud layer, while mostly due to the MF component in the cloud layer. This supports the "mass flux approximation" used in many convective parameterizations that approximate the total flux by the MF component in the cloud layer. The EDMF model represents the residuals as an eddy diffusion process naturally connected with the subcloud layer eddy diffusion, which dominates the flux transport there.

Figures 1e and 1f show the parameters diagnosed from q_t and applied to the chemical tracers. In the cloud layer, the diagnosed ϵ and d are consistent with results in previous studies [e.g., *Siebesma et al.*, 2003]. In the subcloud layer, ϵ and d are smaller, consistent with the relatively constant M in the subcloud layer. K_{qt}, which is close to the results in Figure 11 of *Siebesma et al.* [2003], is very large in the subcloud layer, corresponding to the strong turbulent mixing there that maintains nearly constant vertical profiles of q_t (and other tracers). K_{qt} is small in the cloud layer, corresponding to small ED flux there.

3.1. The Control Case

Now we examine the steady state chemical aspect in the control case of the LES simulations (solid lines in Figure 2). The ϕ_1 profiles (Figure 2a) share similar features with the q_t profiles (Figure 1c), because the source of ϕ_1, like q_t, comes from the surface flux and thus ϕ_1 is well correlated with q_t. $\overline{\phi_1}$ and $\overline{\phi_2}$ are nearly constant with height in the subcloud layer due to the strong turbulent mixing there. ϕ_{1u} and ϕ_{2u} at the cloud base have similar values as $\overline{\phi_1}$ and $\overline{\phi_2}$ in the surface layer, because cloudy updrafts originate from the surface. Above the cloud base, ϕ_{1u} and ϕ_{2u} decrease with height due to the aqueous reaction and entrainment of environmental air having lower mixing ratios. Detrainment of ϕ_2-depleted cloudy air leads to the decrease of $\overline{\phi_2}$ with height. This effect is balanced by the relaxation of ϕ_2 in the clear sky, leading to the intersection of $\overline{\phi_2}$ and ϕ_{2u} at around 800 m height.

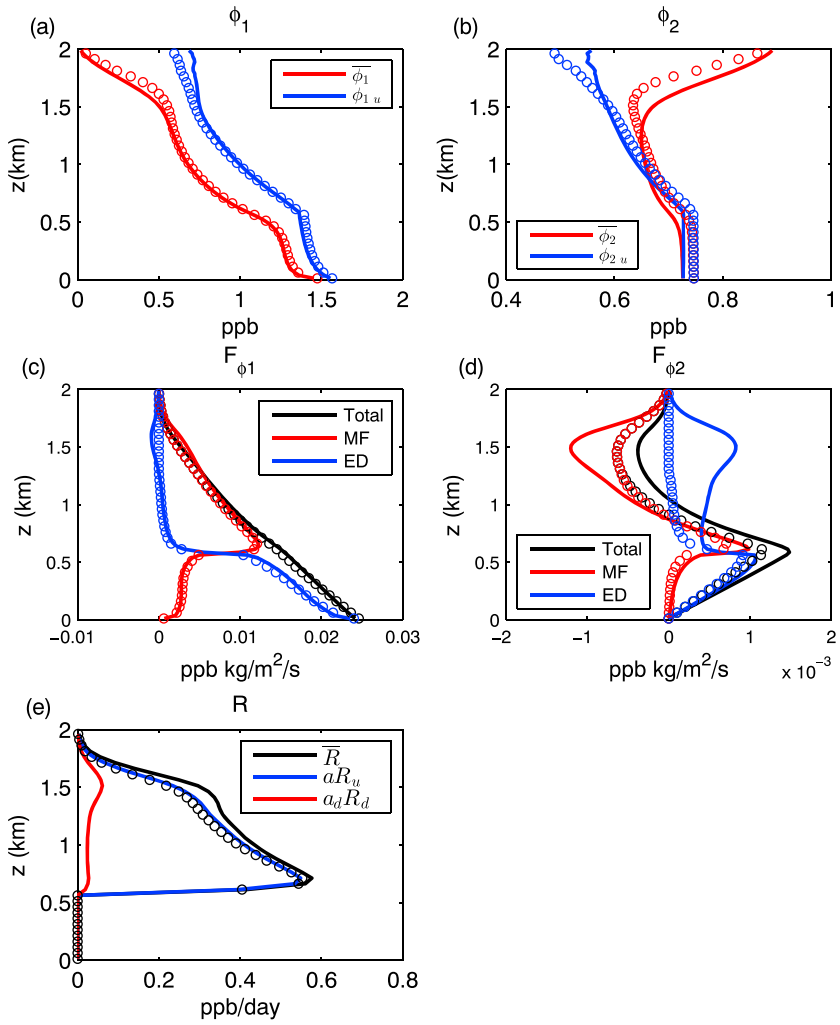

Figure 2. The control case steady state (a) $\overline{\phi_1}$ and ϕ_{1u}, (b) $\overline{\phi_2}$ and ϕ_{2u}, (c) F_{ϕ_1} and its decomposition, (d) F_{ϕ_2} and its decomposition, and (e) aqueous reaction rate and its portion in cloudy updrafts and downdrafts. The color lines are the LES results, and the color circles are the EDMF model results.

The convective fluxes of ϕ_1 and ϕ_2 and their decomposition are shown in Figures 2c and 2d. F_{ϕ_2} is much smaller than F_{ϕ_1} in magnitude due to the small contrast of ϕ_2 in updrafts and environment (Figure 2b). In the subcloud layer, the ED component dominates the total flux of both ϕ_1 and ϕ_2. In the cloud layer, the MF component accounts for almost all of the total flux for ϕ_1. For ϕ_2, the MF and ED components are of comparable amplitudes but with opposite signs. As can be seen from Figures 2c and 2d, the mass flux approximation is well satisfied for ϕ_1, consistent with previous studies that examined the convective transport of surface-originated tracers [e.g., *Vilà-Guerau de Arellano et al.*, 2005]. However, the approximation is not well satisfied for ϕ_2, suggesting that additional considerations are needed for non-surface-originated tracers.

The horizontally averaged reaction rate $\overline{R}$ (Figure 2e) peaks slightly above cloud base and then decreases with height, mainly due to the decrease of cloud fraction with height (Figure 1a). R_u actually increases with height due to the increase of $q_{c,u}$ (figure not shown). Aqueous reaction in cloudy updrafts (aR_u) accounts for most of the total aqueous reaction. Thus, neglecting aqueous reaction in cloudy downdrafts in the EDMF model is an acceptable simplification for the shallow cumulus studied here. For other types of convection with substantial area fraction of cloudy downdrafts, such as stratocumulus, aqueous reaction in cloudy downdrafts should also be considered.

The steady state results of the EDMF model (circles in Figure 2) reproduce the LES results quite well. The matches of ϕ_1 and F_{ϕ_1} are particularly good (vertically averaged relative errors <5%). The EDMF model

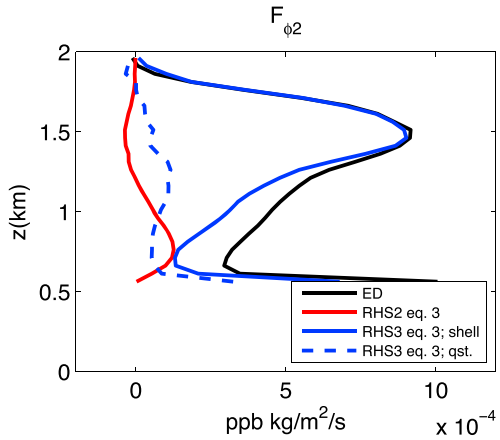

Figure 3. The decomposition of the LES ϕ_2 flux of the "ED" component (black line) into contributions from the cloudy updrafts (red line), the subsiding shells (blue solid line), and the quiescent environment (blue dashed line).

underestimates $\overline{R}$ by about 11%, but this is mostly due to the neglect of the aqueous reaction in cloudy downdrafts. When compared to reactions only in cloudy updrafts (aR_u), the error in EDMF reduces to about 3%. The EDMF model also reproduces ϕ_2 and F_{ϕ_2} (vertically averaged relative errors <5%), although, with some biases in the shape of the profiles. It underestimates the ϕ_2 flux of the MF component in the upper levels and has almost zero ED ϕ_2 flux in the cloud layer. Due to the cancelation of biases, the discrepancies of F_{ϕ_2} between the EDMF and LES results are, fortunately, smaller than discrepancies in the individual components.

Although the EDMF model well reproduces the LES results of the control case, in sections 3.2–3.4 we examine the underlying assumptions of the EDMF model that can lead to errors in representing chemical transports and aqueous reactions and understand the dependence of these errors under different chemical parameters or settings.

3.2. Errors in the Eddy Diffusivity Component

The EDMF model has nonnegligible deficiencies in parameterizing non-surface-originated tracer ϕ_2 (Figures 2b and 2d). Particularly, it has almost zero ED flux component in the cloud layer, due to the small K diagnosed from q_t. Figure 1f also shows K diagnosed from ϕ_1 and ϕ_2. The diffusivities (K) of the surface-originated tracer q_t and ϕ_1 are close to each other. However, K_{ϕ_2} shows quite different features from K_{q_t}.

In the subcloud layer, K_{ϕ_2} is about half of K_{q_t}, but the differences of K there do not affect the EDMF model too much. We have run the EDMF model with K_{q_t} doubled or halved in the subcloud layer. The resulting ϕ_1 and ϕ_2 are very close to the ones shown in Figure 2. This is because in the subcloud layer, K is so large that its first effect is to maintain nearly constant tracer profiles with height. The vertical gradient of tracers is relatively small ($\frac{\partial \psi}{\partial z} \approx 0$). Sizable changes in K can easily be compensated by small adjustments of tracer vertical gradients in the model. The K parameter may be important for the thermodynamic variables (h_l and q_t), which in turn can affect the subcloud layer properties, such as the subcloud layer depth and the delicate convective inhibition near the cloud base. However, for passive chemical tracers that do not interact with convection, using K diagnosed from q_t is sufficient for parameterizing them in the subcloud layer.

In the cloud layer, K_{ϕ_2} has a singular point near the 1300 m level, corresponding to the local minimum of $\overline{\phi_2}$ there (Figure 2b). Above that level, K_{ϕ_2} is negative, which is unphysical. Note that the "ED" flux in the LES (Figure 2d) is actually calculated as the difference between the total flux and the flux due to the MF component. As seen from equations (3)–(4), the EDMF model posits that $\rho a\overline{w'\psi'}^u + \rho(1-a)\overline{w'\psi'}^e \approx -\rho K_\psi \frac{\partial \overline{\psi}}{\partial z}$, under the assumptions that $\rho a\overline{w'\psi'}^u$ is small and the turbulence in the environment is random. Figure 3 shows that $\rho a\overline{w'\phi_2'}^u$ is relatively small. The positive ϕ_2 flux of the ED component (and thus the negative K_{ϕ_2}) is mostly due to transport in the subsiding shells (Figure 3), which is defined here as grids within 200 m of the nearest cloudy updrafts edge, including both saturated and unsaturated air [*Heus and Jonker*, 2008]. The flux in the rest of the environment (quiescent environment) is very small. If we further increase the cloud shell size, for example, to within 400 m of the updrafts edge, the ϕ_2 flux in the quiescent environment becomes slightly negative and follows the ϕ_2 gradient as eddy diffusion. The above analysis suggests that for

non-surface-originated tracer ϕ_2, the eddy diffusion cannot appropriately represent the non-MF component flux, and the subsiding shells of the shallow cumulus clouds should be included in the parameterization.

3.3. Errors Due To In-Cloud Heterogeneities

Next, we move to the MF component (i.e., the bulk plume model) of the EDMF model, particularly the aqueous reaction rate in the cloud layer. The bulk plume model assumes that the environment and cloudy updrafts have uniform properties within each category (the top-hat approximation) [*Siebesma and Cuijpers*, 1995]. In other words, the bulk plume model explicitly distinguishes cloudy updrafts from the environment but neglects the heterogeneities of air within cloudy updrafts and the environment, leading to errors in the calculation of the aqueous reaction. To estimate the relative importance of the heterogeneity within cloudy updrafts, we define a segregation error (γ_{seg}, with units of percent) as the relative error due to the top-hat approximation when the cloudy updraft mean properties are correctly predicted,

$$\gamma_{\text{seg}} = \frac{\phi_{1u}\,\phi_{2u}\,q_{c,u} - \overline{\phi_{1,n}\phi_{2,n}q_{c,n}}^{c}}{\overline{\phi_{1,n}\phi_{2,n}q_{c,n}}^{c}}. \tag{10}$$

Neglecting second-order terms, γ_{seg} can be written as

$$\gamma_{\text{seg}} \approx -C_{\phi_1,q_c}\mu_{\phi_1}\mu_{q_c} - C_{\phi_2,q_c}\mu_{\phi_2}\mu_{q_c} - C_{\phi_1,\phi_2}\mu_{\phi_1}\mu_{\phi_2}, \tag{11}$$

where $C_{x,y}$ is the correlation coefficient between x and y and μ_x is the coefficient of variation (the ratio of the standard deviation to the mean) of x. γ_{seg} with the opposite sign is very close to the intensity of segregation used in many previous studies [e.g., *Krol et al.*, 2000; *Vilà-Guerau de Arellano et al.*, 2005]. Here the segregation of tracers in clear-sky and cloudy updrafts is already taken into account in the bulk plume model, so that γ_{seg} measures segregation of tracers inside cloudy updrafts.

The decomposition of γ_{seg} in the LES control case based on equation (11) is shown in row 1 of Figure 4. First, we examine the correlation coefficients in Figure 4 (row 1, middle column). ϕ_1 is strongly positively correlated with q_c in cloudy updrafts (C_{ϕ_1,q_c} is close to 1), as expected. ϕ_2 and q_c are also positively correlated near the cloud base, implying that the most energetic subcloud-layer updrafts are enriched in the reactive tracers and moisture. As cloudy updrafts rise, the aqueous reaction of the reactive tracers with each other leads to the negative correlation between ϕ_1 and ϕ_2. In addition, above the height where ϕ_{2u} and $\overline{\phi_2}$ intersect (around 800 m, Figure 2b), entrainment has opposite effects on ϕ_2 and ϕ_1 of cloud updrafts: it increases ϕ_2 but decreases ϕ_1 in cloud updrafts. As a result, C_{ϕ_1,ϕ_2} (and also C_{ϕ_2,q_c}) becomes more and more negative as the updrafts go up. μ_{q_c} is large near cloud base (the upper right column) is because $q_{c,u}$ is small. μ_{ϕ_1} and μ_{ϕ_2} are much smaller than μ_{q_c}, indicating that reaction in the control case is slow and leads to very weak heterogeneities of ϕ_1 and ϕ_2 in cloudy updrafts. The upper left column plots the products of the correlation coefficients and coefficients of variation (i.e., the RHS terms of equation (11)). In the control case, γ_{seg} is dominated by the RHS1 term (the covariance between ϕ_1 and q_c) because the in-cloud heterogeneity of ϕ_1 (μ_{ϕ_1}) is larger than that of ϕ_2 (μ_{ϕ_2}).

As the relative abundances of ϕ_1 and ϕ_2 change in experiments in group 1, the reaction timescale and strength of in-cloud heterogeneities of the reactive tracers also change. The decompositions of γ_{seg} for a ϕ_1-dominant case (the case with $\phi_{2,\text{ref}}/\phi_{2,\text{ref0}} = 1/12$ and $\overline{\phi_1} \approx 400\overline{\phi_2}$) and a ϕ_2-dominant case (the case with $\phi_{2,\text{ref}}/\phi_{2,\text{ref0}} = 12$ and $\overline{\phi_2} \approx 500\overline{\phi_1}$) are shown in rows 2 and 3 of Figure 4, respectively. Compared to the control case, the correlation coefficients are qualitatively similar in all three cases, but μ_{ϕ_1} and μ_{ϕ_2} can vary significantly. When ϕ_1 is strongly dominant in cloudy updrafts, ϕ_2 reacts quickly and thus has a short lifetime. The fast reaction leads to low values and strong in-cloud heterogeneities of ϕ_2, giving the large value of μ_{ϕ_2} (blue line in the right column of row 2), even though its updraft mean value is small. As a result, γ_{seg} is dominated by the covariance term between ϕ_2 and q_c (RHS2 term, blue line in the left column of row 2). When ϕ_2 is strongly dominant in cloudy updrafts, based on the same argument, γ_{seg} is dominated by the covariance term between ϕ_1 and q_c (RHS1 term, red line in the left column of row 3).

We can define a Damköhler number (D_a) [e.g., *Molemaker and Vilà-Guerau de Arellano*, 1998; *Krol et al.*, 2000; *Schumann*, 1989] as the ratio of the in-cloud residence time of air parcels in shallow convection (τ_{con}) to the reaction timescale (τ_{ϕ_1} and τ_{ϕ_2}) to characterize the influences of convection on the aqueous reaction,

$$D_{a,\phi_{1,2}} = \frac{\tau_{\text{con}}}{\tau_{\phi_{1,2}}}. \tag{12}$$

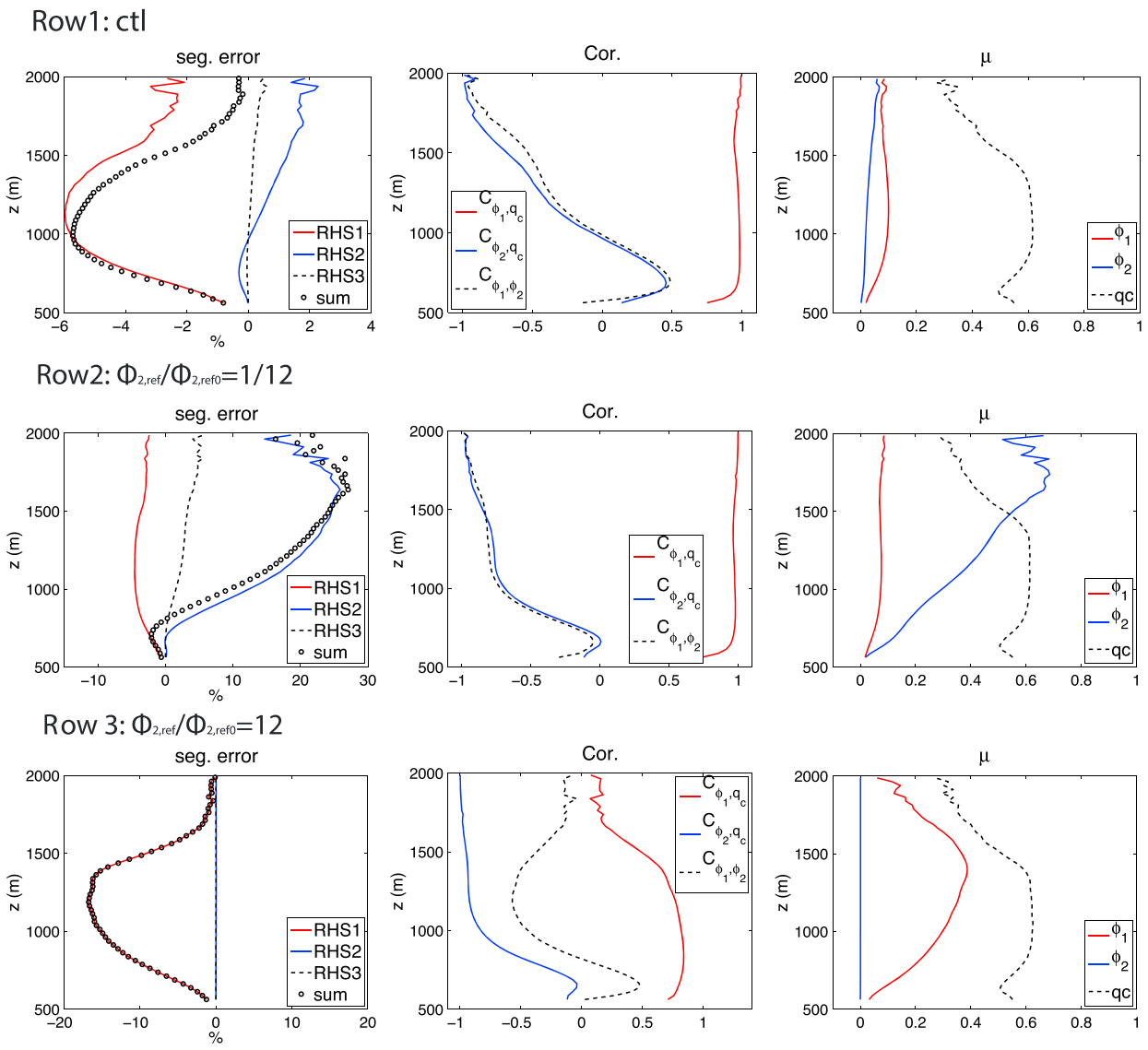

Figure 4. (left column) The segregation error and its decomposition based on equation (11). (middle column) The correlation coefficients between ϕ_1, ϕ_2, and q_c in cloudy updrafts. (right column) The coefficients of variation of ϕ_1, ϕ_2, and q_c. From row 1 to row 3, they are for the control case, $\phi_{2,\mathrm{ref}}/\phi_{2,\mathrm{ref0}} = 1/12$ case, and $\phi_{2,\mathrm{ref}}/\phi_{2,\mathrm{ref0}} = 12$ case, respectively.

D_a being far smaller than 1 indicates that the heterogeneity of reactive tracers in cloudy updrafts is small, and the updraft mean is adequate for the calculation of reaction rate. D_a being close to or greater than 1 indicates that the segregation of reactive tracers in cloudy updrafts is significant and may need to be taken into account.

τ_{con} can be estimated by dividing the total cloudy air mass by total inflow,

$$\tau_{\mathrm{con}} = \frac{\int_{z_{cb}}^{z_{ct}} a\rho \mathrm{d}z}{M(z_{cb}) + \int_{z_{cb}}^{z_{ct}} \epsilon M \mathrm{d}z}. \tag{13}$$

Using ϵ_{qt}, this gives $\tau_{\mathrm{con}} = 370$ s. Alternatively, *Neggers et al.* [2002] calculated the eddy turnover time of individual clouds as the cloud depth is divided by the cloud-averaged maximum vertical velocity. They found that the BOMEX clouds with different cloud depths have a relatively constant eddy turnover time of about 400 s (see their Figure 4), close to τ_{con} estimated here by equation (13). Note that τ_{con} can be much smaller than the Òlife time of a cumulus cloud ($\sim 10^3$ s), because a cumulus cloud is continuously fed with updrafts

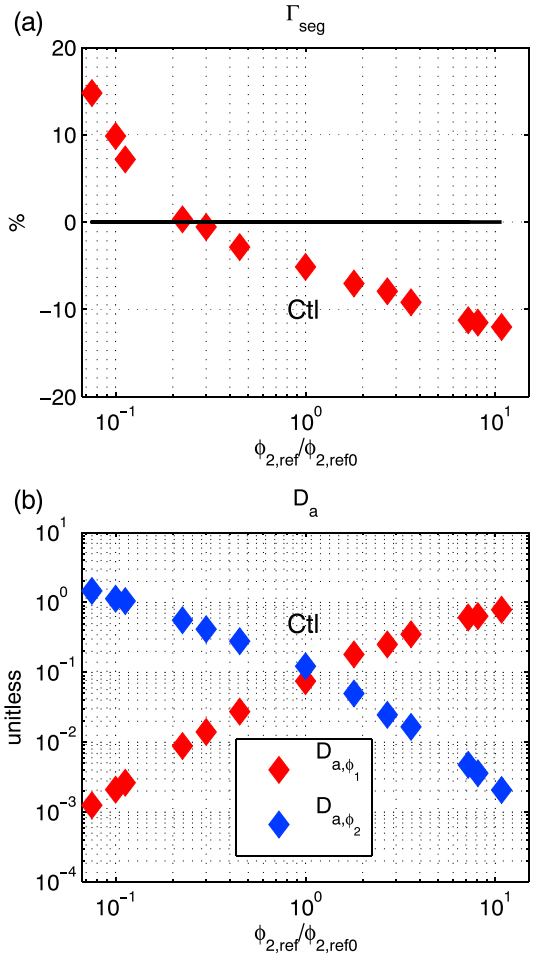

Figure 5. (a) Γ_{seg} and (b) D_{a,ϕ_1} and D_{a,ϕ_2} of the cases in group 1.

from subcloud layer. The reaction timescale of ϕ_1 in the cloud layer as a whole can be estimated as the total ϕ_1 is divided by the total reaction rate in cloudy updrafts,

$$\tau_{\phi_1} = \frac{\int_{z_{cb}}^{z_{ct}} a\rho\phi_{1u}\mathrm{d}z}{\int_{z_{cb}}^{z_{ct}} a\rho R_u \mathrm{d}z}. \tag{14}$$

τ_{ϕ_2} can be estimated in a similar way. The reaction timescale on a particular level may differ from the overall timescale estimated from equation (14). For the control case, this gives $\tau_{\phi_1} \approx 5 \times 10^3$ s and $\tau_{\phi_2} \approx 3 \times 10^3$ s.

To represent the overall segregation error in the cloud layer, we define Γ_{seg} as the vertically averaged γ_{seg} weighted by the product of the cloudy updraft fraction and density. Γ_{seg} and the D_a of reactive tracers for all cases in group 1 are summarized in Figure 5. From left to right, the reaction regime changes from ϕ_1 dominant to ϕ_2 dominant. Correspondingly, D_{a,ϕ_1} changes from $\sim 10^{-3}$ to ~ 1, and D_{a,ϕ_2} changes from ~ 1 to $\sim 10^{-3}$ (Figure 5b). Γ_{seg} is dominated by the covariances between q_c and the tracer with the smaller reaction timescale (larger D_a). Thus, Γ_{seg} is positive to the left end and negative to the right end. In either direction, the absolute value of Γ_{seg} increases as the larger D_a value between the two reactive tracers increases. As the larger D_a approaches and exceeds 1, which indicates that the reaction timescale is close to or faster than the in-cloud residence timescale, in-cloud heterogeneities have greater impacts on the aqueous reaction, but errors are only about 10% when $D_a \approx 1$. In the real atmosphere, in situations in which the SO_2 concentration dominates the H_2O_2 concentration, O_3 may take in charge and play a bigger role in the aqueous oxidation of SO_2, resulting in reduced segregation between SO_2 and oxidants in cloudy updrafts.

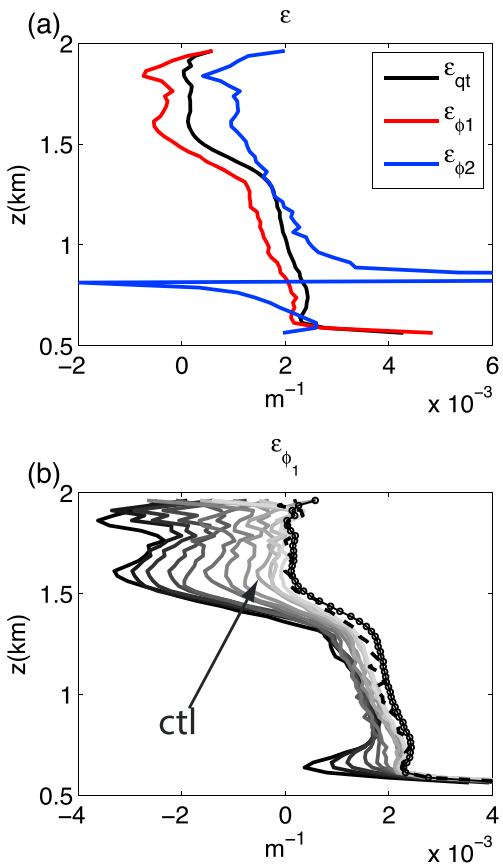

Figure 6. (a) The control case ϵ_{q_t}, ϵ_{ϕ_1}, and ϵ_{ϕ_2} that are diagnosed from their conservation equations. (b) Each line indicates ϵ_{ϕ_1} of one case in group 2. Lines from lighter to darker are cases from small k (10^{-4}) to large k (10^{-1}). The dashed line corresponds to $k = 0$ case. ϵ_{q_t} is also plotted as circle for reference.

3.4. Errors Due To Entrainment/Detrainment Rates

The dependence of entrainment/detrainment rates (ϵ/d) on tracers can lead to errors in the EDMF model. For q_t and h_l, because they are so well correlated, their ϵ/d are almost identical [e.g., *Siebesma et al.*, 2003]. However, ϵ_{ϕ_1} and ϵ_{ϕ_2} diagnosed from the LES results show sizable differences from ϵ_{q_t} for the control case (Figure 6a). Since ϵ and d are constrained by the mass flux equation (equation (5), i.e., $\epsilon_{\phi_1} - d_{\phi_1} = \epsilon_{q_t} - d_{q_t}$), here we only focus on the discussion of ϵ. Because the reaction is slow in the control case ($D_{a,\phi_{1,2}} \approx 0.1$), the surface-originated tracer ϕ_1 has ϵ similar to but slightly smaller than ϵ of q_t. The intersection of ϕ_{2u} and $\overline{\phi_2}$ around 800 m (Figure 2b) leads to the unrealistic oscillation and negative values of ϵ_{ϕ_2} around that height. The tracer dependence on ϵ is largely due to the aqueous reaction. The actual detrained (entrained) air seldom has the cloudy updraft mean (environmental mean) properties [*Romps*, 2010; *Dawe and Austin*, 2011; *Nie and Kuang*, 2012b]. Because of the aqueous reaction, the differences between $\phi_{1,2}$ in detrained cloudy updrafts and their mean values in the cloudy updrafts are different from those of q_t. Thus, detraining (entraining) the same amount of cloudy (environmental) air leads to different fractional changes of the environmental (bulk plume) $\phi_{1,2}$ and q_t.

We estimate the errors of R due to the tracer dependence of ϵ in the bulk plume model as follows. The bulk plume (equations (5) – (6)) starts at cloud base with $\phi_{1,u}$ and $\phi_{2,u}$ diagnosed from LES. After integrating upward over each level, we calculate γ_{seg} on that level from the LES results with equation (11) and use it to correct R_u. With the errors due to in-cloud heterogeneities fixed, what is left of the errors of R_u is only due to the errors in the cloudy updrafts mean tracer values caused by the inaccurate ϵ/d. The bulk plume model is integrated to the cloud top. The relative differences between the resulting R_u and the LES R_u are vertically averaged with the weighting factor of a and density, giving an estimation of entrainment error (Γ_{ent}, with units of percent). Because ϕ_{2u} and $\overline{\phi_2}$ are very close to each other (Figure 2b), the differences between ϵ_{q_t} and ϵ_{ϕ_2} have little

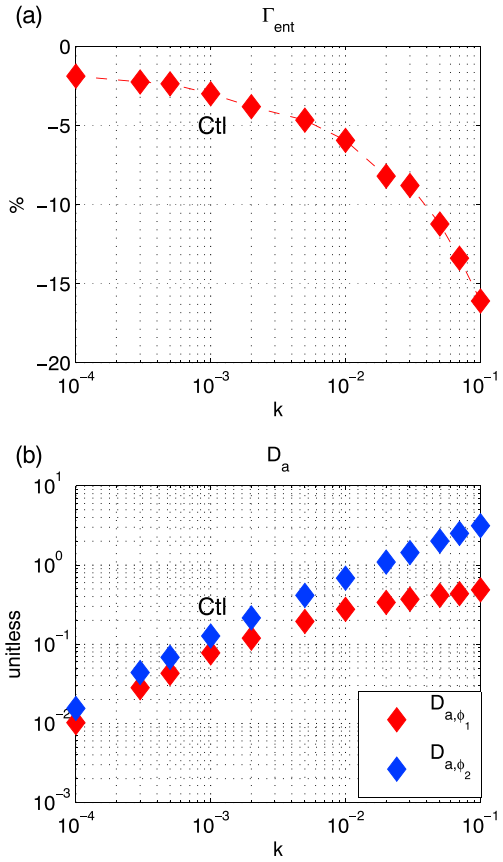

Figure 7. (a) Γ_{ent} and (b) D_{a,ϕ_1} and D_{a,ϕ_2} of the cases in group 2.

effect on the calculation of ϕ_{2u}. Analyses indicate that Γ_{ent} is dominated by the differences between ϵ_{ϕ_1} and ϵ_{q_t}; therefore, our discussions hereafter focus on ϕ_1 and ϵ_{ϕ_1}.

It is expected that Γ_{ent} is also related to D_a. As long as the reaction timescale is large compared to the in-cloud residence timescale ($D_a \ll 1$), reactive tracers behave similarly to conservative tracers and Γ_{ent} should be small. When the reaction timescale is close to or smaller than the in-cloud residence timescale, the aqueous reaction will have larger effects on ϵ, leading to larger Γ_{ent}. The cases in group 2, in which we vary k from 10^{-4} to 10^{-1}, demonstrate the above argument. Figure 6b shows the ϵ_{ϕ_1} for all cases in group 2. As k increases, ϵ_{ϕ_1} deviates farther away from ϵ_{q_t} to more negative values. Figure 7 shows Γ_{ent} and D_a of the group 2 cases as a function of k. As k increases from 10^{-4} to 10^{-1}, D_{a,ϕ_1} increases from $\sim 10^{-2}$ to $\sim 10^{-1}$ and D_{a,ϕ_2} from $\sim 10^{-2}$ to ~ 1. Consistently, as D_a increases and approaches 1, the absolute value of Γ_{ent} starts to increase sharply (Figure 7a). Γ_{ent} is always negative because ϵ_{ϕ_1} is always smaller than ϵ_{q_t} due to the aqueous reaction.

The analyses in sections 3.3 and 3.4 show that for most of the cases examined, the aqueous reaction can be viewed as slow ($D_a \ll 1$) compared to convective timescale. Thus, errors in the aqueous reaction due to segregation and the dependence of entrainment/detrainment rates on tracers are small. The EDMF model with diagnosed parameters from q_t reproduces the transport and reactions of ϕ_1 and ϕ_2 quite well.

3.5. Evaluating the Operator-Splitting Error in CTMs

In this subsection, we evaluate the error due to operator splitting that is used in many CTMs. This is done by running the EDMF model but with the transport and aqueous reaction calculated separately over a typical CTM time step, as introduced in section 2.3.

Figure 8 summarizes the mean tracer concentrations (vertically averaged from the surface to the cloud top level) and mean aqueous reaction rate (vertically averaged from the cloud base to the cloud top level) in all the cases in the two groups. We first examine the LES results in group 1 (Figures 8a–8c), in which the relative ratio between ϕ_1 and ϕ_2 decreases moving from left to right on the x axes. The dependence of $\overline{\phi_1}$ and $\overline{\phi_2}$ on

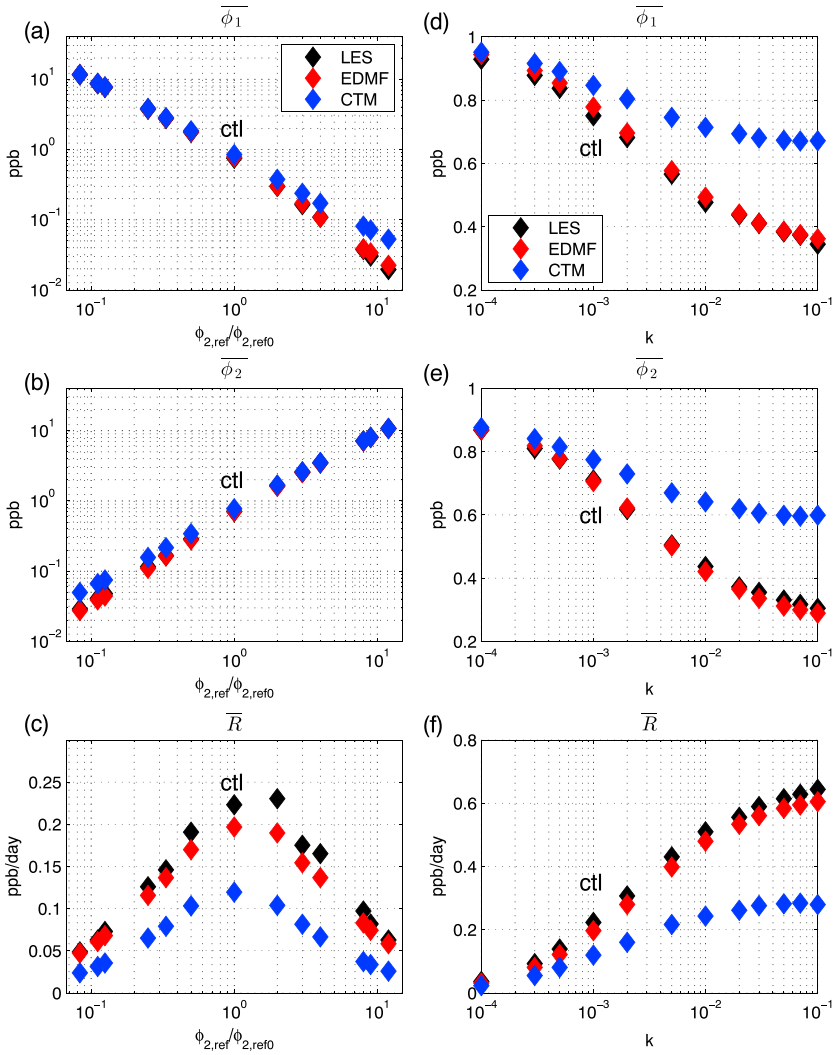

Figure 8. From Figures 8a–8f, each panel shows the LES (black), the EDMF model (red), and the EDMF model with operator-splitting (blue) results of the (a and d) vertical averaged $\overline{\phi_1}$, (b and e) $\overline{\phi_2}$, and (c and f) $\overline{R}$, respectively. Figures 8a–8c are for the cases in group 1, and Figures 8d–8f are for the cases in group 2.

the relative abundance of ϕ_1 and ϕ_2 (x axes) is consistent with the experiment designs (note that the y axes in Figures 8a and 8b are logarithmic). Figure 8c shows that the LES $\overline{R}$ peaks when ϕ_1 and ϕ_2 are comparable in cloudy updrafts. The cases in group 2 (Figures 8d–8f) show that as k increases, both $\overline{\phi_1}$ and $\overline{\phi_2}$ decrease, while $\overline{R}$ increases.

The EDMF model results (red markers in Figure 8) match the LES results quite well for the three variables in all the cases. However, if the transport and aqueous reaction in the EDMF model are treated as separated operators as is done in many CTMs over ΔT_{CTM} (30 min in the calculation shown in Figure 8), the results (blue markers) show significant error. To provide a quantitative estimation of the errors, Figure 9 shows the normalized root-mean-square errors (NRMSEs) of $\overline{\phi_1}$, $\overline{\phi_2}$, and $\overline{R}$ for all cases in the two EDMF model settings. The open markers indicate that the mean is underestimated by simple models, while the solid markers indicate that the mean is overestimated. Consistent with previous analysis, when ϕ_2 becomes dominant (D_{a,ϕ_1} approaches 1), the NRMSE of $\overline{\phi_1}$ increases (Figure 9a). The opposite holds when ϕ_1 becomes dominant (Figure 9b). For the second group of experiments (Figures 9d–9f), as k increases, D_{a,ϕ_1} and D_{a,ϕ_2} approach 1, consistent with the increases of the NRMSEs. In all the cases, the error in the EDMF model is much greater if the transport and aqueous reaction are treated as separated operators than if they are calculated simultaneously.

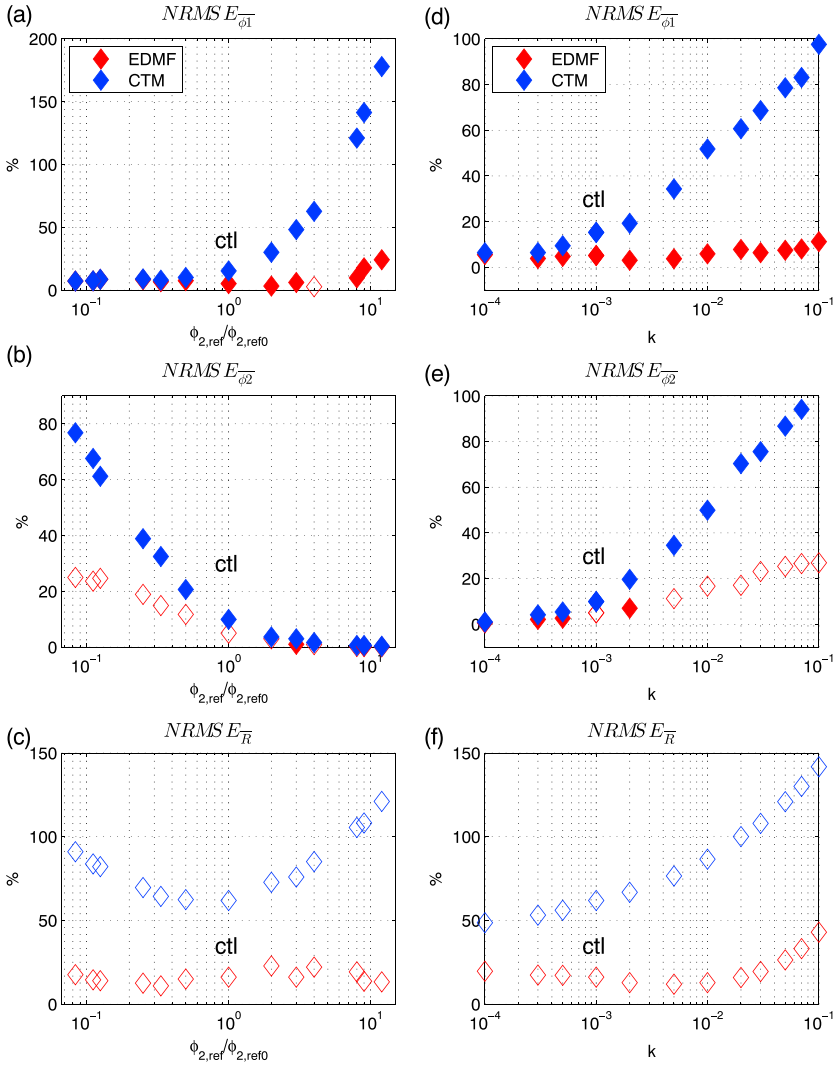

Figure 9. The NRMSE of (a and d) $\overline{\phi_1}$, (b and e) $\overline{\phi_2}$, and (c and f) $\overline{R}$ of the results of the EDMF model (red) and the EDMF model with operators splitting (blue). Solid (open) marker indicates that the vertical averaged variables are overestimated (underestimated) by the simple model compared to the LES results. Figures 9a–9c are for the cases in group 1, and Figures 9d–9f are for the cases in group 2.

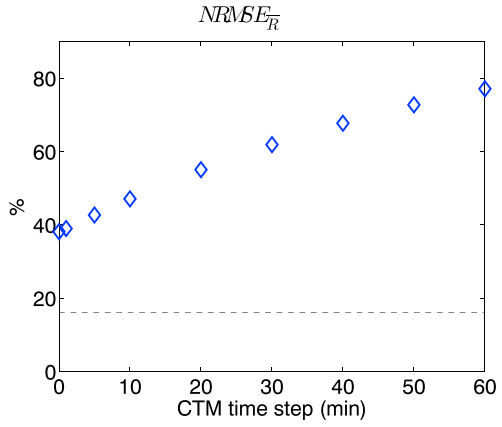

Figure 10. The control case NRMSE of $\overline{R}$ in the EDMF model with operators splitting as functions of ΔT_{CTM}. The dashed line indicates NRMSE of $\overline{R}$ in the EDMF model with tracer transport and aqueous reactions calculated simultaneously.

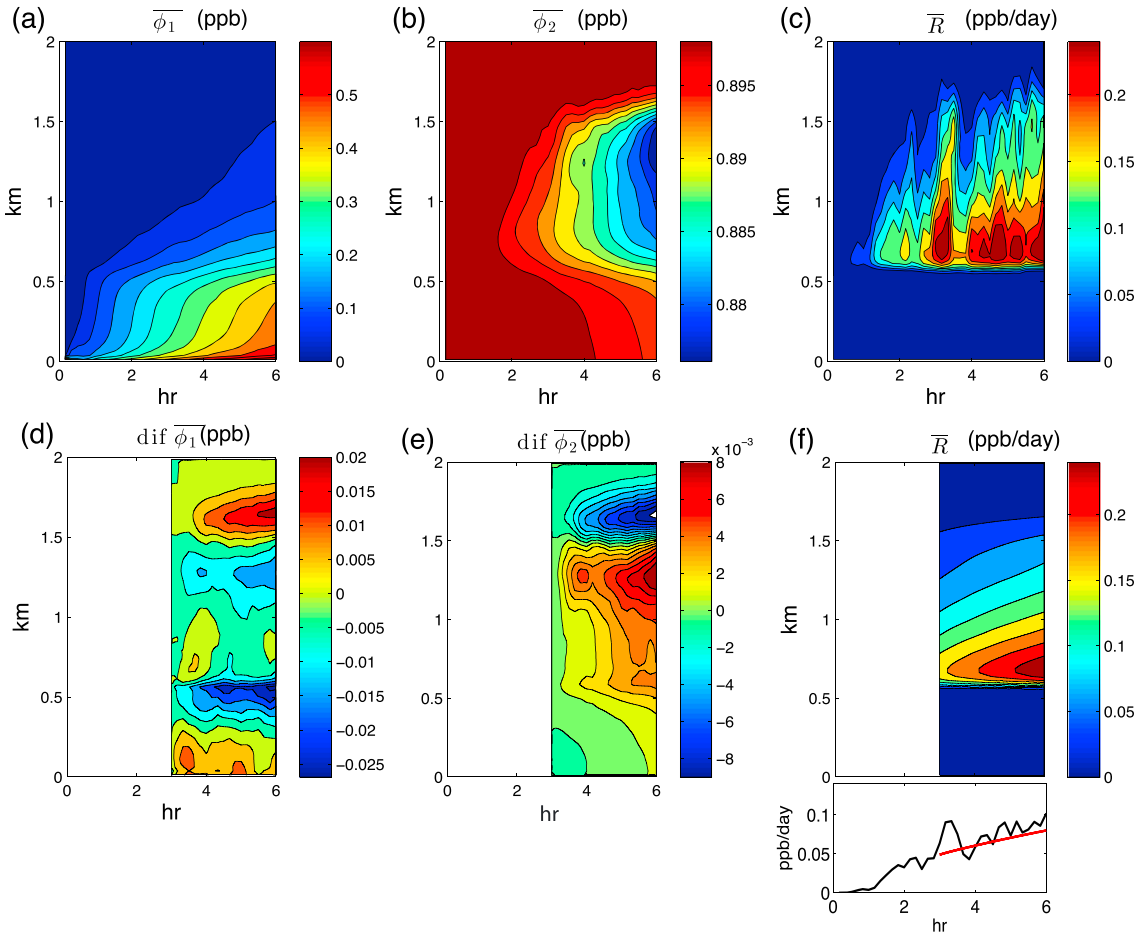

Figure 11. The comparison between the LES and EDMF model in the transient case with $k = 10^{-3}$. (a–c) The time evolution of $\overline{\phi_1}$, $\overline{\phi_2}$, and $\overline{R}$ of the LES results, respectively. (d and e) Differences of $\overline{\phi_1}$ and $\overline{\phi_2}$ between the EDMF model and the LES results, respectively. (f) The time evolution of $\overline{R}$ of the EDMF model results (top) and the vertically averaged time series of $\overline{R}$ of the EDMF model (red line) and LES results (black line) (bottom).

The errors due to operator splitting decreases as ΔT_{CTM} decreases (Figure 10, taking the control case as an example). However, even if ΔT_{CTM} decreases to 4 s, the same of the sub-CTM time step, operator splitting still leads to additional errors.

Although here we evaluate the errors due to the operator splitting in CTMs using the EDMF model, this error is independent of the EDMF model and exists in other mass flux-based convective parameterizations. On the other hand, a mass flux-based convective parameterization can reduce this error by calculating tracer transport and aqueous reactions in updrafts simultaneously [e.g., *Berg et al.*, 2015].

3.6. Chemical Transient States

Although the above analyses are in chemical steady states, the EDMF model with diagnosed parameters also works well in transient states. In the following three transient cases ($k = 0,\ 10^{-3},\ 10^{-1}$), the BOMEX case is initialized from hour 0 and runs for 6 h. The initial conditions of chemical tracers are ϕ_1 being zero and ϕ_2 being the reference value.

Figures 11a–11c show the LES-simulated evolution of tracer profiles and reaction rate of the $k = 10^{-3}$ case. As time progresses, ϕ_1 builds up in the subcloud layer and is transported upward by convective updrafts. The aqueous reaction leads to the decrease of ϕ_2 in the cloudy layer, and the ϕ_2-depleted air is entrained into the subcloud layer and decreases $\overline{\phi_2}$ there. $\overline{R}$ becomes nonnegligible at about hour 0.5 and continues to grow, due to the development of shallow cumuli and the building up of ϕ_1. During the thermodynamical steady period (hour 3 to hour 6), there is considerable variability of cloud fraction, reflected as the variation of $\overline{R}$. This internal variability, however, can be reduced by increasing the LES domain size or averaging over an ensemble of simulations.

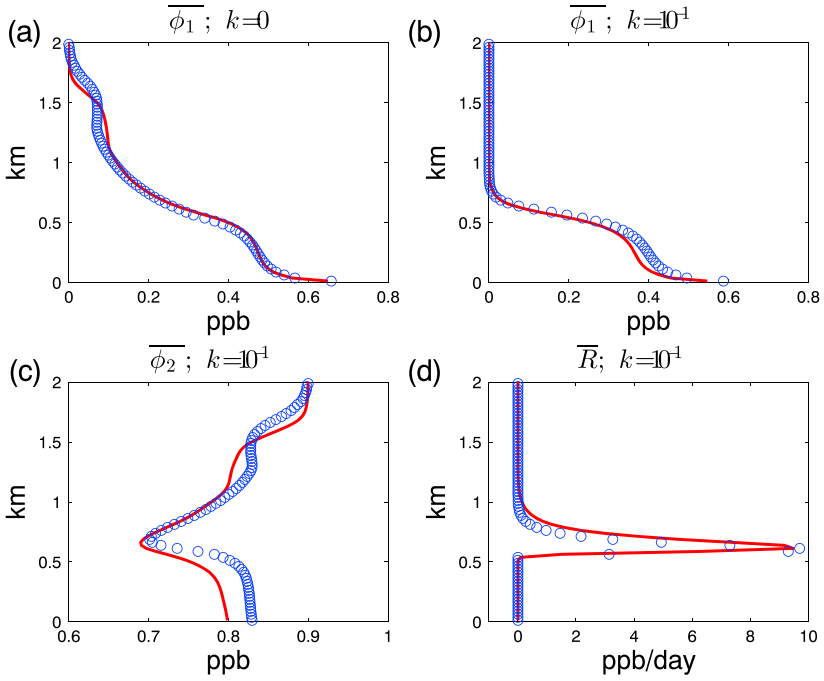

Figure 12. The hour 6 profiles of (a) $\overline{\phi_1}$ of the $k = 0$ case; (b) $\overline{\phi_1}$, (c) $\overline{\phi_2}$, and (d) $\overline{R}$ of the $k = 10^{-1}$ case. The red solid lines are the LES results, and the blue circles are the EDMF model results.

We run the EDMF model from hour 3 to hour 6, with the same entrainment/detrainment and the same eddy diffusivity parameters as the ones in previous subsections. The initial profiles of the reactive tracers are taken from the LES profiles at hour 3. The differences of $\overline{\phi_1}$ and $\overline{\phi_2}$ between the EDMF model and the LES results (Figures 11d and 11e) are small. $\overline{R}$ in the EDMF results shows smoother variation in time than it does in the LES results (color contour in Figure 11f). The comparison of vertically averaged $\overline{R}$ between the EDMF model and the LES (Figure 11f) shows that the EDMF model captures the LES results well. Figure 12 shows the comparison of the hour 6 profiles from the LES and the EDMF model (which also starts from hour 3) for the $k = 0$ and $k = 10^{-1}$ cases. Without aqueous reaction ($k = 0$), more ϕ_1 is transported into cloudy layer (Figure 12a). With strong aqueous reaction ($k = 10^{-1}$), significant amounts of ϕ_1 are only found in the subcloud layer (Figure 12b), since ϕ_1 in cloudy updrafts quickly reacts near the cloud base (Figure 12d). In both cases, the EDMF model reasonably reproduces the LES results.

4. Conclusions and Discussions

The goal of this study is to improve the representation of aqueous phase reactions in shallow cumuli in global models. An LES with an idealized chemical reaction mimicking the aqueous oxidation of surface-originated SO_2 by H_2O_2 is used to guide simple models. We show that the EDMF approach with a bulk plume model is a promising solution. When entrainment/detrainment rates and eddy diffusivity are diagnosed using a conservative thermodynamic tracer (e.g., q_t), the EDMF model represents the transport and aqueous reactions of reactive tracers quite well over a wide range of parameters. The eddy diffusion component of the EDMF model is sufficient for parameterizing surface-originated chemical tracers, while it may neglect the tracer transport in the cloud shells for non-surface-originated tracers. The bulk plume component of the EDMF approach has two sources of errors: neglecting the heterogeneities within cloudy updrafts leads to a segregation error between reactive tracers and cloud water and the use of entrainment/detrainment parameters derived from q_t on reactive tracers leads to an entrainment error. Both of these errors are related to the reaction timescale. When the reaction is slow compared to the in-cloud residence time of air parcels, the reactive tracers behave like conservative tracers, so that the EDMF model that represents the conservative thermodynamic tracers well can also represent the reactive tracers well. When the reaction timescale approaches the in-cloud residence time of air parcels, in-cloud heterogeneity increases and the entrainment/detrainment rates of reactive tracers further deviate from those derived using conserved variables, resulting in greater errors.

The errors due to operator splitting are estimated by running the EDMF model in a CTM-like configuration where the tracer transport and aqueous reactions are calculated separately over a time step representative of CTMs, and the aqueous reaction calculations use horizontal mean (rather than updraft) tracer concentrations. The error due to operator splitting can be significant (>50% for all cases examined here with a CTM time step of 30 min), especially when the reaction is fast compared to the in-cloud residence time. The error decreases as the CTM time step decreases but remains larger than that of the case with tracer transport and aqueous reactions calculated simultaneously in the cloudy updrafts.

In this study, the parameters for the EDMF model are diagnosed from a conserved thermodynamical tracer. In GCMs, the uncertainties in these parameters, and therefore the parameterized convection, are still the leading source of errors for the representation of atmospheric chemistry. However, these uncertainties may be reduced by diagnosing convective parameters from the resolved convection of a cloud-resolving model inside each GCM column, a method known as the super-parameterized GCMs [*Grabowski*, 2001; *Khairoutdinov and Randall*, 2001]. *Gustafson et al.* [2008] and *Wang et al.* [2011] have already adopted this approach and applied it in aerosol-climate simulations. In this study, we lend support to theirs, provide an evaluation of the approach in an idealized setting, and analyze the sources of errors and their dependence on chemical reaction regimes.

Although a bulk plume model is used in the EDMF model in this study, many convection parameterizations use multiple plumes/parcels to represent cloudy updrafts [e.g., *Berg and Stull*, 2005; *Nie and Kuang*, 2012a; *Sušelj et al.*, 2013]. A multiple plume/parcel representation allows heterogeneities within cloudy updrafts, which can improve the representation of nonlinear microphysical processes [e.g., *Krueger et al.*, 1997; *Nie and Kuang*, 2012b; *Tölle and Krueger*, 2014]. It can also potentially benefit the aqueous reactions by, for example, accounting for the segregation between reactive tracers in cloudy updrafts and having different entrainment/detrainment rates for each plume.

The current work focuses on the a nonprecipitating shallow cumulus convection with an idealized aqueous reaction. Future work is needed to include more realistic chemistry, additional complexities in convection (e.g., precipitation, downdrafts, and convective organization), and their possible interactions (aerosol-cloud interaction) [e.g., *Berner et al.*, 2013; *Wyant et al.*, 2015; *Berg et al.*, 2015].

Acknowledgments
The authors thank Jessica Kunke for improving writing of the manuscript. Comments from Mary Barth and two anonymous reviewers substantially improved the paper. The numerical simulations presented were obtained and stored on the Harvard Odyssey cluster. The data can be accessed upon contacting the authors (jn2460@columbia.edu). J.N. acknowledges support from the Lamont Postdoctoral Fellowship. Z.K. acknowledges support from NSF grants AGS-1062016 and AGS-1260380 and the Office of Biological and Environmental Research of the U.S. Department of Energy under grant DE-SC0008679 as part of the ASR program.

References

Alexander, B., R. J. Park, D. J. Jacob, Q. B. Li, R. M. Yantosca, J. Savarino, C. C. W. Lee, and M. H. Thiemens (2005), Sulfate formation in sea-salt aerosols: Constraints from oxygen isotopes, *J. Geophys. Res.*, *110*, D10307, doi:10.1029/2004JD005659.

Barth, M. C., P. J. Rasch, J. T. Kiehl, C. M. Benkovitz, and S. E. Schwartz (2000), Sulfur chemistry in the National Center for Atmospheric Research Community Climate Model: Description, evaluation, features, and sensitivity to aqueous chemistry, *J. Geophys. Res.*, *105*, 1387–1415, doi:10.1029/1999JD900773.

Benkovitz, C. M., S. E. Schwartz, M. P. Jensen, and M. A. Miller (2006), Attribution of modeled atmospheric sulfate and SO2 in the Northern Hemisphere for June–July 1997, *Atmos. Chem. Phys.*, *6*, 4723–4738.

Berg, L. K., and R. B. Stull (2005), A simple parameterization coupling the convective daytime boundary layer and fair-weather cumuli, *J. Atmos. Sci.*, *62*, 1976–1988.

Berg, L. K., C. M. Berkowitz, J. C. Barnard, G. Senum, and S. R. Springston (2011), Observations of the first aerosol indirect effect in shallow cumuli, *Geophys. Res. Lett.*, *38*, L03809, doi:10.1029/2010GL046047.

Berg, L. K., M. Shrivastava, R. C. Easter, J. D. Fast, E. G. Chapman, Y. Liu, and R. A. Ferrare (2015), A new WRF-Chem treatment for studying regional-scale impacts of cloud processes on aerosol and trace gases in parameterized cumuli, *Geosci. Model Dev.*, *8*, 409–429.

Berner, A. H., C. S. Bretherton, R. Wood, and A. Muhlbauer (2013), Marine boundary layer cloud regimes and POC formation in an LES coupled to a bulk aerosol scheme, *Atmos. Chem. Phys.*, *13*, 12,549–12,572.

Daum, P. H., T. J. Kelly, S. E. Schwartz, and L. Newman (1984), Measurements of the chemical composition of stratiform clouds, *Atmos. Environ.*, *18*, 2671–2684.

Dawe, J. T., and P. H. Austin (2011), The influence of the cloud shell on tracer budget measurements of LES cloud entrainment, *J. Atmos. Sci.*, *68*, 2909–2920.

Easter, R. C., S. J. Ghan, Y. Zhang, R. D. Saylor, E. G. Chapman, N. S. Laulainen, H. Abdul-Razzak, L. R. Leung, X. Bian, and R. A. Zaveri (2004), MIRAGE: Model description and evaluation of aerosols and trace gases, *J. Geophys. Res.*, *109*, D20210, doi:10.1029/2004JD004571.

Ghan, S. J., X. Liu, R. C. Easter, R. Zaveri, P. J. Rasch, J.-H. Yoon, and B. Eaton (2012), Toward a minimal representation of aerosols in climate models: Comparative decomposition of aerosol direct, semidirect, and indirect radiative forcing, *J. Climate*, *25*, 6461–6476.

Grabowski, W. W. (2001), Coupling cloud processes with the large-scale dynamics using the cloud-resolving convection parameterization (CRCP), *J. Atmos. Sci.*, *58*, 978–997.

Gustafson, W. I., L. K. Berg, R. C. Easter, and S. J. Ghan (2008), The explicit-cloud parameterized-pollutant hybrid approach for aerosol cloud interactions in multiscale modeling framework models: Tracer transport results, *Environ. Res. Lett.*, *3*(2), 025005.

Heus, T., and H. J. J. Jonker (2008), Subsiding shells around shallow cumulus clouds, *J. Atmos. Sci.*, *65*, 1003–1018.

Holland, J. Z., and E. M. Rasmusson (1973), Measurement of atmospheric mass, energy, and momentum budgets over a 500-kilometer square of tropical ocean, *Mon. Weather Rev.*, *101*, 44–55.

Jacob, D. J., et al. (1997), Evaluation and intercomparison of global atmospheric transport models using Rn-222 and other short-lived tracers, *J. Geophys. Res.*, *102*, 5953–5970.

Jacob, P., T. M. Tavares, V. C. Rocha, and D. Klockow (1990), Atmospheric H2O2 field measurements in a tropical environment: Bahia, Brazil, *Atmos. Environ.*, *124A*, 377–382.
Jöckel, P., et al. (2006), The atmospheric chemistry general circulation model ECHAM5/MESSy1: Consistent simulation of ozone from the surface to the mesosphere, *Atmos. Chem. Phys.*, *6*, 5067–5104.
Kazil, J., H. Wang, G. Feingold, A. D. Clarke, J. R. Snider, and A. R. Bandy (2011), Modeling chemical and aerosol processes in the transition from closed to open cells during VOCALS-REx, *Atmos. Chem. Phys. Discuss.*, *11*, 7491–7514.
Khairoutdinov, M. F., and D. A. Randall (2001), A cloud-resolving model as a cloud parameterization in the NCAR Community Climate System Model: Preliminary results, *Geophys. Res. Lett.*, *28*, 3617–3620.
Khairoutdinov, M. F., and D. A. Randall (2003), Cloud-resolving modeling of the ARM summer 1997 IOP: Model formulation, results, uncertainties and sensitivities, *J. Atmos. Sci.*, *60*, 607–625.
Kim, S. W., M. C. Barth, and M. Trainer (2012), Influence of fair-weather cumulus clouds on isoprene chemistry, *J. Geophys. Res.*, *117*, D10302, doi:10.1029/2011JD017099.
Koehler, M. (2005), Improved Prediction of Boundary Layer Clouds, *ECMWF Newsletter*, vol. 104, pp. 18–22, ECMWF, Reading, United Kingdom.
Krol, M. C., M. J. Molemaker, and J. Vila-Guerau (2000), Effects of turbulence and heterogeneous emissions in photochemically active species in the convective boundary layer, *J. Geophys. Res.*, *105*, 6871–6884.
Krueger, S. K., C. Su, and P. A. McMurtry (1997), Modeling entrainment and finescale mixing in cumulus clouds, *J. Atmos. Sci.*, *54*, 2697–2712.
Lawrence, M. G., and J. R. Philip (2005), Tracer transport in deep convective updrafts: Plume ensemble versus bulk formulations, *J. Atmos. Sci.*, *62*, 2880–2894.
Liu, X., J. E. Penner, and M. Herzog (2005), Global modeling of aerosol dynamics: Model description, evaluation, and interactions between sulfate and nonsulfate aerosols, *J. Geophys. Res.*, *110*, D18206, doi:10.1029/2004JD005674.
Molemaker, M. J., and J. Vilà-Guerau de Arellano (1998), Control of chemical reactions by convective turbulence in the boundary layer, *J. Atmos. Sci.*, *55*, 568–579.
Neggers, R. A. J., A. P. Siebesma, and H. J. J. Jonker (2002), A multiparcel model for shallow cumulus convection, *J. Atmos. Sci.*, *69*, 1655–1668.
Nie, J., and Z. Kuang (2012a), Responses of shallow cumulus convection to large-scale temperature and moisture perturbations: A comparison of large-eddy simulations and a convective parameterization based on stochastically entraining parcels, *J. Atmos. Sci.*, *69*, 1936–1956.
Nie, J., and Z. Kuang (2012b), Beyond bulk entrainment and detrainment rates: A new framework for diagnosing mixing in cumulus convection, *Geophys. Res. Lett.*, *39*, L21803, doi:10.1029/2012GL053992.
Rasch, P. J., M. C. Barth, J. T. Kiehl, S. E. Schwartz, and C. M. Benkovitz (2000), A description of the global sulfur cycle and its controlling processes in the National Center for Atmospheric Research Community Climate Model, Version 3, *J. Geophys. Res.*, *105*, 1367–1385.
Romps, D. M. (2010), A direct measure of entrainment, *J. Atmos. Sci.*, *67*, 1908–1927.
Sakugawa, H., I. R. Kaplan, W. Tsai, and Y. Cohen (1990), Atmospheric hydrogen peroxide, *Environ. Sci. Technol.*, *24*, 1452–1462.
Schumann, U. (1989), Large-eddy simulation of turbulent diffusion with chemical reactions in the convective boundary layer, *Atmos. Environ.*, *23*, 1713–1727.
Seinfeld, J. H., and S. N. Pandis (1998), *Atmospheric Chemistry and Physics: From Air Pollution to Climate Change*, p. 366, John Wiley, New Jersey.
Siebesma, A. P., and J. W. M. Cuijpers (1995), Evaluation of parametric assumptions for shallow cumulus convection, *J. Atmos. Sci.*, *52*, 650–666.
Siebesma, A. P., et al. (2003), A large eddy simulation intercomparison study of shallow cumulus convection, *J. Atmos. Sci.*, *60*, 1201–1219.
Siebesma, A. P., P. M. M. Soares, and J. Teixeira (2007), A combined eddy diffusivity mass flux approach for the convective boundary layer, *J. Atmos. Sci.*, *64*, 1230–1248.
Sušelj, K., J. Teixeira, and G. Matheou (2012), Eddy diffusivity/mass flux and shallow cumulus boundary layer: An updraft PDF multiple mass flux scheme, *J. Atmos. Sci.*, *69*, 1513–1533.
Sušelj, K., J. Teixeira, and D. Chung (2013), A unified model for moist convective boundary layers based on a stochastic eddy-diffusivity/mass-flux parameterization, *J. Atmos. Sci.*, *70*, 1929–1953.
Tölle, M. H., and S. K. Krueger (2014), Effects of entrainment and mixing on droplet size distributions in warm cumulus clouds, *J. Adv. Model. Earth Syst.*, *6*, 281–299.
Verma, S., O. Boucher, M. S. Reddy, H. C. Upadhyaya, P. Le Van, F. S. Binkowski, and O. P. Sharma (2007), Modeling and analysis of aerosol processes in an interactive chemistry general circulation model, *J. Geophys. Res.*, *112*, D03207, doi:10.1029/2005JD006077.
Vilà-Guerau de Arellano, J., S.-W. Kim, M. C. Barth, and E. G. Patton (2005), Transport and chemical transformations influenced by shallow cumulus over land, *Atmos. Chem. Phys.*, *5*, 3219–3231.
Wang, M., et al. (2011), The multi-scale aerosol-climate model PNNL-MMF: Model description and evaluation, *Geosci. Model Dev.*, *4*, 137–168.
Wu, S., L. J. Mickley, D. J. Jacob, J. A. Logan, R. M. Yantosca, and D. Rind (2007), Why are there large differences between models in global budgets of tropospheric ozone?, *J. Geophys. Res.*, *112*, D05302, doi:10.1029/2006JD007801.
Wyant, M. C., et al. (2015), Global and regional modeling of marine boundary layer clouds and aerosols in the marine boundary layer during VOCALS: The VOCA intercomparison, *Atmos. Chem. Phys.*, *15*, 153–172.